Materials Characterization 203 (2023) 113124

Contents lists available at ScienceDirect

Materials Characterization

journal homepage: www.elsevier.com/locate/matchar

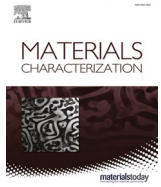

In-situ XRD investigation of σ phase precipitation kinetics during isothermal holding in a hyper duplex stainless steel

Roman Schuster [a,*], Andreas Keplinger [b], Aurélie Jacob [a], Johannes Kreyca [c], Laszlo Solyom [d], Emad Maawad [e], Erwin Povoden-Karadeniz [a,d]

[a] Christian Doppler Laboratory for Interfaces and Precipitation Engineering CDL-IPE, Institute of Materials Science and Technology, TU Wien, Getreidemarkt 9, 1060 Vienna, Austria
[b] voestalpine BÖHLER Edelstahl GmbH & Co KG, Mariazeller Straße 25, 8605 Kapfenberg, Austria
[c] voestalpine Stahl Donawitz GmbH, Kerpelystraße 199, 8700 Leoben, Austria
[d] Institute of Materials Science and Technology, TU Wien, Getreidemarkt 9, 1060 Vienna, Austria
[e] Institute of Materials Physics, Helmholtz-Zentrum Hereon, Max-Planck-Strasse 1, Geesthacht D-21502, Germany

ARTICLE INFO

Keywords:
Duplex steel
Sigma phase
In-situ XRD experiments
Microstructure characterization
Precipitation mechanism
Austenite ferrite interface

ABSTRACT

The precipitation kinetics and formation mechanisms of σ phase during isothermal holding of a hyper duplex stainless steel in the temperature range from 750 °C to 1025 °C were studied by means of in-situ high energy X-ray diffraction experiments. Rietveld analysis of the data determined the nose temperature as 900 °C where a σ phase fraction of 1 wt% is attained after 15 s. The measurements revealed a distinct change from initial interface controlled nucleation of σ phase to a later stage of diffusion controlled growth during holding at 1000 °C after the σ phase fraction reaches half its final value. At lower holding temperatures the change from interface control to diffusion control happens more gradual and at later stages of the transformation. At these lower temperatures σ phase precipitation is accompanied by the formation of secondary austenite. Changes in σ phase formation mechanisms and kinetics were correlated with variations in the morphology of the precipitates through SEM analysis of quenched samples. Isothermal holding at 1000°C and 1025 °C as well as above the solvus temperature of σ phase at 1120 °C leads to local fluctuations of austenite and ferrite phase fractions and the concomitant movement of austenite/ferrite phase boundaries even when no overall change in the phase fractions occurs.

1. Introduction

Duplex stainless steels with about equal fraction of austenite and ferrite offer attractive mechanical and corrosion resistance properties. They possess higher strength than austenitic steels and better corrosion resistance than ferritic steels [1]. To achieve a duplex steel microstructure, significant concentrations of both ferrite stabilizing elements, mainly Cr and Mo and secondarily Si, as well as austenite stabilizing elements such as Ni, Mn, N or Cu need to be added. To further enhance the mechanical and corrosion resistance properties higher alloyed super and hyper duplex stainless steels were developed [2]. Due to the high alloying content and the chemical heterogeneities at ferrite austenite boundaries, thermo-mechanical processing below the solutionizing temperature may lead to the precipitation of intermetallic phases, nitrides or carbides [3–7]. The formation of the intermetallic σ phase is of particular significance since it precipitates fast, can grow to significant volumes and leads to deterioration of mechanical properties and corrosion resistance of the steel [4,8–10].

Previous work on the precipitation of σ phase in duplex steels (e.g. [6,11]) has shown that σ phase can precipitate at ferrite/austenite phase boundaries, ferrite grain boundaries as well as in ferrite grains through a eutectoid reaction, where ferrite transforms to σ phase and secondary austenite. Continued growth of σ phase precipitates, that nucleated at grain or phase boundaries, may be accompanied with the formation of secondary austenite between σ phase precipitates [8,12]. In highly alloyed hyper duplex steels formation of noticeable quantities of σ phase precipitates were reported after <60 s of isothermal holding. The morphology of σ phase precipitates varies with the temperature during formation, where lower temperatures lead to finer morphologies due to slower diffusion of σ phase forming elements in ferrite [6,8,11].

In this context, precise characterization of the kinetics of σ phase formation is necessary for a comprehensive understanding of the com-

* Corresponding author.
E-mail address: roman.schuster@tuwien.ac.at (R. Schuster).

https://doi.org/10.1016/j.matchar.2023.113124
Received 31 March 2023; Received in revised form 23 June 2023; Accepted 24 June 2023
Available online 30 June 2023

plex transformation processes in this high-alloyed steel system. This paper focuses on the in-situ measurements of the kinetics of σ phase formation during isothermal holding in a hyper duplex stainless steel. Previous simulation and experimental studies determined different nose temperatures between 936 °C and 950 °C [13–15]. The experimental studies were performed using electron microscopy analysis of quenched samples, which limits the precision of the time resolution of the precipitation process particularly in the early stages of σ phase formation.

Consequently, we performed in-situ X-ray diffraction experiments during isothermal holding at temperatures between 750 °C and 1025 °C utilizing high energy synchrotron radiation with high beam brilliance to track the formation of σ phase. The main advantages of this method over conventional investigations of quenched samples are the high time resolution necessary due to the very fast kinetics of the σ phase formation in hyper duplex steels, the opportunity to track the evolution of the phase fraction development in the same sample over the whole heat treatment, and the elimination of possible quenching effects. Similar in-situ X-ray studies using low energy radiation have been performed on lower grade duplex steels with slower kinetics of σ phase formation, determining the kinetics of formation and dissolution of σ phase during isothermal holding [16,17]. These studies revealed shortcomings of experimental studies relying on conventional ex-situ σ phase characterization performed on quenched samples. Our experiments using high energy X-rays allow us to determine the σ phase formation kinetics in hyper duplex stainless steel (HDSS) with exceptional time resolution in large sample volumes and also avoid distortion by surface effects that occur in low energy X-ray experiments. In addition, we performed ex-situ quenching experiments to observe the variations of σ phase morphologies resulting from changing σ phase formation mechanisms at different holding temperatures and times.

2. Materials and methods

2.1. Material

The rolled HDSS samples investigated in this study were produced at voestalpine BÖHLER Edelstahl. The steel has the same chemical composition as the steel investigated by Jacob and Povoden-Karadeniz [18] (Table 1). Optical micrographs of the samples in the as received state reveal the typical microstructure found in rolled duplex steels (Fig. 1). The duplex microstructure consists of layered austenite elongated in the rolling direction with a width of about 5 µm surrounded by a ferrite matrix. The dilatometer samples were machined to cylinders with 4 mm diameter and 10 mm height, so that the long axis of the cylinder was parallel to the elongation direction of the austenite domains.

The equilibrium phase fraction distribution including austenite, ferrite, σ phase and Cr_2N were calculated for the investigated HDSS alloy based on the Calphad assessment of the hyper duplex stainless steel compositional system, using a refined version of the Matcalc steel database mc_fe. [19]. The calculations show that the ferrite and austenite phase fractions become equal at about 1000 °C, and σ phase forms below about 1050 °C (Fig. 2).

2.2. In-situ diffraction experiments

The in-situ high temperature diffraction experiments were performed at the High Energy Materials Science beamline (P07b) operated by the Helmholtz-Zentrum Hereon at the PETRA III storage ring of DESY in Hamburg, Germany [20]. The heat treatments were conducted with a modified Bähr 805A/D dilatometer, that allows to perform transmission XRD experiments during the aging experiments. The samples were held between two quartz rods in the induction heating solenoid under vacuum. The temperature was controlled through S-type thermocouples spot-welded to the sample adjacent to the measured sample volume. The beam direction during the in-situ experiments was orthogonal to the sample long axis and therefore orthogonal to the austenite elongation direction. For the aging experiments all samples were initially heated to 1120 °C at a rate of 25 K/s. After holding at 1120 °C for 5 min the samples were cooled with 50 K/s to the respective isothermal holding temperature between 750 °C and 1025 °C, where they were held for 2000 s. The samples were then quenched to 40 °C. The thermocouple data demonstrated that the actual temperature in the vicinity of the beam shows only minute deviations from the set temperature.

The X-ray measurements were conducted with a monochromatic X-

Table 1
Chemical composition of the investigated steel in wt%.

C	Cr	Ni	Mo	Cu	Mn	N	Si	Fe
<0.01	26.3	6.9	4.6	0.2	2.9	0.37	0.2	Bal.

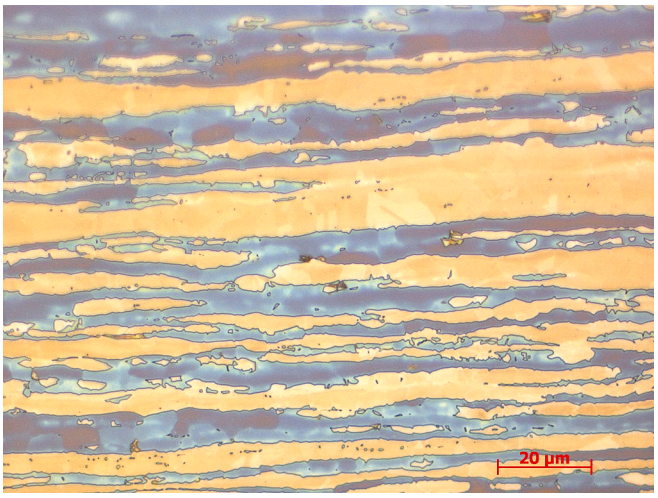

Fig. 1. Optical micrograph of an etched sample showing the as received microstructure consisting of about 5 µm thick austenite domains (yellow) surrounded by ferrite (blue) in about equal proportions. The image corresponds to a section normal to the beam direction in the diffraction experiments. The electrochemical etching was performed with a mixture of 5 parts distilled water and 2 parts NaOH at 1.3 V for 5 s. (For interpretation of the references to colour in this figure legend, the reader is referred to the web version of this article.)

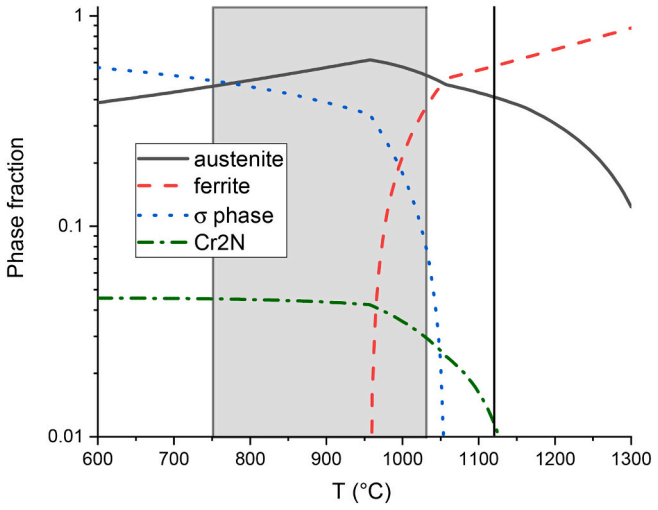

Fig. 2. Computed Calphad-based equilibrium phase fractions as function of temperature of the investigated HDSS showing the stability range of σ phase. The temperature range of the isothermal holding experiments is marked by the gray area. The solutionizing temperature is marked by a black line. (modified after Jacob and Povoden-Karadeniz [18]).

ray beam with 87.1 keV photon energy with a spot size of 700 × 700 μm on the sample. Diffraction patterns were recorded every 4 s with a 2D Perkin Elmer XRD 1621 flat panel detector at a distance of about 1390 mm from the sample. To measure the detector background noise, dark current images were recorded with every diffraction pattern. This set-up allowed to record the full Debye Scherrer rings up to 2θ angles of 12° corresponding to a wave vector of about 9.2 $Å^{-1}$. A secondary photon energy of 174.2 keV with a far lower beam brilliance leads to another set of Bragg peaks at half the diffraction angle of the peaks from the primary beam energy (Fig. 3). These secondary Bragg peaks do not overlap with the primary Bragg peaks used in the further analysis. During the heating experiments X-ray measurements were taken for 1 s with a delay of about 3.17 s between the individual measurements, resulting in 480 measurements during the 2000s long isothermal holding sections.

2.3. Evaluation of X-ray data

The 2D diffraction patterns were integrated over the full Debye Scherrer rings with the software Fit2D [21] to obtain 1D diffraction profiles. The 2θ range between 1.7 and 11 ° was used for the evaluation. This range excludes the strongest reflections produced by the 174.2 keV photons at low angles as well as only partially recorded Debye-Scherrer rings at the edge of the detector. The calibration of the sample to detector distance and detector tilt angle was performed using the diffraction pattern of an untextured LaB^6 powder sample recorded under the same conditions as the HDSS diffraction patterns. Fig. 3b shows two integrated profiles from sample HD800 at different stages of the heating experiment. Direct analysis of the diffraction profiles was performed with the software Fityk [22], in order to check the quality of the integration and to observe the evolution of Bragg reflections. Phase analysis and Rietveld refinement were performed with the software Highscore Plus from the company Malvern Panalytical [23]. For the Rietveld analysis lattice parameters, phase fraction and peak shape functions were independently refined for each diffractogram using one set of starting parameters for all measurements performed at the same holding temperature. The background parameters were constant for all measurements. This set-up allows to evaluate the evolution of the phase fractions and the lattice parameters during isothermal holding with a time resolution of about 4.17 s, while minimizing systematic deviations between the measurements.

2.4. Ex-situ analysis

Short term holding experiments were performed with an equivalent Bähr 805A/D dilatometer at the Institute of Materials Science and Technology at the TU Wien, Austria. The heat treatments were identical to the in-situ experiments except that the holding times at 900 °C were 25, 50 and 75 s and at 1000 °C 600 s instead of 2000 s. Additionally, longer holding experiments were performed at 750 °C for 3500 s and at 1000 °C for 5000 s to measure the phase fraction distribution after the ferrite dissolution. Subsequent SEM analysis was performed with a Zeiss Sigma 500 VP SEM located at the Institute of Materials Science and Technology at the TU Wien.

Electron probe microanalysis (EPMA) on 15 σ phase precipitates in the samples held at 900 °C for 75 s and at 1000 °C for 600 s was performed using a CAMECA SX Five Field-Emission-Gun Electron Microprobe (CAMECA–Ametec, Gennevilliers, France) at the Faculty of Geosciences, Geography, and Astronomy at the University of Vienna (Austria). An accelerating voltage of 15 kV, a beam current of 20 nA and a working distance of 10 mm were used.

3. Results

3.1. X-ray profile analysis

Analysis of the X-ray profiles reveals that σ phase precipitates during isothermal holding at all investigated temperatures between 750 and 1025 °C and the austenite phase fraction increases at the expense of the ferrite fraction after cooling from 1120 °C (Table 2). Significant Bragg reflections that are not consistent with either austenite, ferrite or σ phase are not observed, indicating that the fraction of other phases that may form at these temperatures such as Cr_2N or χ phase are secondary to σ phase. The evolution of the austenite Bragg peaks reveals two distinct temperature regimes. At holding temperatures $\leq$ 950 °C the austenite peaks develop prominent right shoulders coinciding with the emergence of σ phase peaks (Fig. 4). These shoulders are interpreted as pertaining to secondary austenite generated by the reaction $\alpha \rightarrow \sigma + \gamma$ which has a smaller lattice parameter than the original austenite due to a different chemical composition than the original austenite, leading to overlapping peaks from the original austenite fraction and the emerging secondary austenite. Therefore, austenite peaks were fitted by two face-centered cubic (fcc) phases with different lattice parameters in the Rietveld analysis. The austenite fraction corresponding to the original chemical composition is here referred to as γ_a. The evolution of γ_a during the heating experiments is due to changes of the main austenite Bragg reflections. The fraction with the smaller lattice parameter emerging during the isothermal holding is referred to as γ_b. The γ_b fraction evolution is due the emergence and growth of the right shoulders of the austenite Bragg reflections. Modeling the Bragg reflections with Pseudo-Voight functions in the Rietveld refinement allows to distinguish the

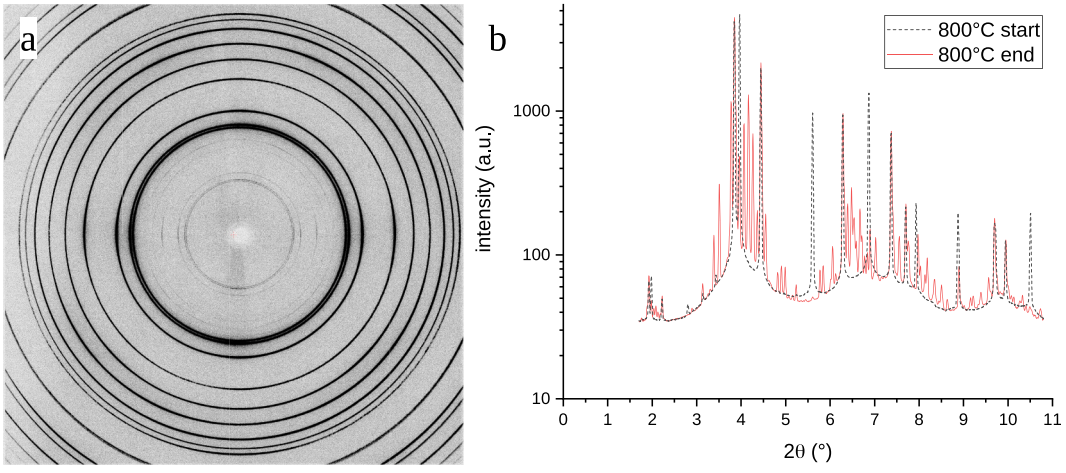

Fig. 3. (a) 2D XRD diffraction patterns of the initial microstructure obtained at room temperature. (b) Integrated 1D diffraction profiles at the start and end of isothermal holding at 800 °C.

Table 2
Sample list showing phase fractions in wt% at the start and end of the isothermal holding as well as the equilibrium phase fractions calculated with MatCalc including ferrite, austenite, σ phase and Cr_2N using a refined version of the Matcalc steel database mc_fe [19].

Name	T(°C)	Start holding		End holding			Calculated			
		α	γ	α	γ	σ	α	γ	σ	Cr_2N
HD750	750	55	45	12.9	60.6	26.6	0	46	49	5
HD800	800	47.3	52.7	0	62.5	37.5	0	49	46	4
HD850	850	52.4	47.6	0	61.6	38.5	0	53	43	4
HD900	900	53.2	46.8	0.3	65.1	34.6	0	57	39	4
HD950	950	48.9	51.1	0.3	65.9	33.7	0	61	35	4
HD1000	1000	53.6	46.4	8.6	64.9	26.5	22	57	18	4
HD1025	1025	55.3	44.7	49.7	48.8	1.5	47	49	2	3

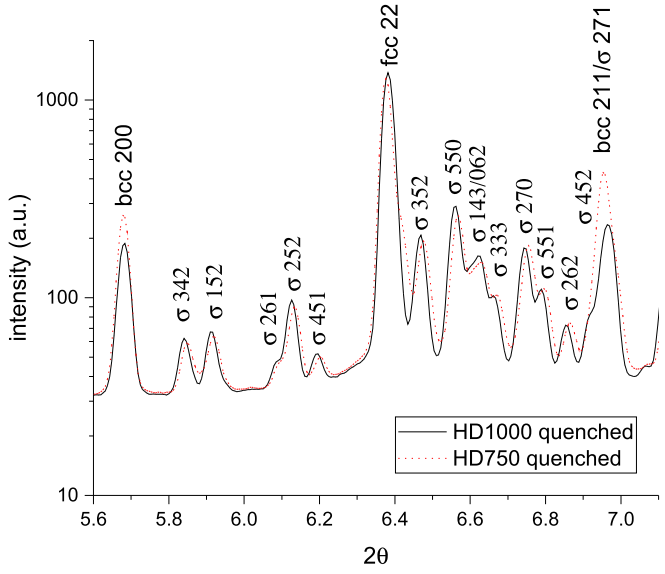

Fig. 4. X-ray profiles of samples held at 750 °C (red) and 1000°C (black) in the 2θ range between 5.6 and 7.1° after quenching to 40 °C. The austenite and ferrite peaks are labeled as fcc and bcc, respectively. The 220 austenite peak shows a pronounced right shoulder at 750 °C. The σ phase peaks at 750 °C are shifted to higher angles compared to 1000 °C. (For interpretation of the references to colour in this figure legend, the reader is referred to the web version of this article.)

peak areas of the two austenite fractions. This permits to track the evolution of γ_a and γ_b separately. The overall austenite fraction γ_{sum} is the sum of γ_a and γ_b. In the high temperature regime with holding temperatures of 1000 and 1025 °C the γ_b fraction is negligible. Here $\gamma_a \simeq \gamma_{sum}$.

3.2. Isothermal holding

The evolution of ferrite, austenite and σ phase fractions during isothermal holding was quantified by applying Rietveld analysis to the diffraction profiles and is discussed in the following. Fig. 5a shows the phase fraction evolution during holding at 800 °C, which is typical for the lower temperature regime ($\leq$ 950 °C). At these temperatures the growth of σ phase begins to slow down when the α fraction has decreased below about 10 wt%. In the samples held at temperatures from 800 °C to 950 °C ferrite is almost completely consumed during the 2000 s long isothermal holding (Table 3). The fastest growth of σ phase occurs at 900 °C (Fig. 6). The time-temperature precipitation diagram for σ phase calculated from the Rietveld analysis results shows that at 900 °C 1% and 90% of the final σ phase fraction are reached after 9 s and 127 s, respectively (Fig. 7). For holding temperatures from 800 °C to 950 °C 90% of the final σ phase fraction is reached within 500 s (Fig. 7). The growth of σ phase in the lower temperature regime (T $\leq$ 950 °C) is accompanied by an increase of the γ_{sum} fraction. While the early growth of γ during isothermal holding pertains to the γ_a fraction, during the growth of σ phase at the expense of α, the increase in γ is due to the formation of γ_b. Once the α fraction is below about 1 wt%, the σ phase and γ_b fractions continue to grow slightly at the expense of γ_a. The fraction of γ_b at the end of the holding treatment generally increases with increasing temperature from 750 to 950 °C, while the difference between the lattice parameters of γ_a and γ_b decreases with increasing temperature in this temperature range. The γ_b lattice parameter is about 0.6% smaller than the γ_a lattice parameter at 750 °C. This difference is about 0.5, 0.5, 0.4, and 0.2% for 800, 850, 900 and 950 °C, respectively.

During holding at 1000 °C, the formation of σ phase slows down after about 500 s when the α fraction is still ~20% (Fig. 5b). For the rest of the holding time the σ phase fraction increases much slower and linearly from 17% to 26.5% after 2000 s. The decrease of the ferrite phase fraction coincides with a decrease in the ferrite lattice parameter, which ends after about 800 s of holding, when the decrease of the ferrite phase fraction slows considerably (Fig. 8). While the formation of σ phase is accompanied by an increase of γ also at 1000 °C this is due to an increase of γ_a while no significant fraction of γ_b is observed. Before the onset of σ phase formation the γ and α fractions exhibit a slightly oscillating evolution. Once a significant fraction of σ phase has formed, the evolution of the γ and α fractions continues smoothly as during holding at lower temperatures. Increasing the holding temperature to 1025 °C greatly delays the formation of σ phase and the σ phase fraction reaches only 1.5 wt% after 2000 s (Fig. 5c). The austenite and ferrite fractions exhibit an undulating behavior during the holding treatment that is more pronounced than at 1000 °C. The ferrite fraction decreases from initially 56% until an approximately even fraction of austenite and ferrite is reached after about 100 s. While no substantial long term change in this fraction occurs during the 2000 s holding, the ferrite fraction fluctuates between 49 and 54% (Fig. 5c). This undulating evolution of the austenite and ferrite phase fractions occurs also during the solutionizing treatment at 1120 °C before isothermal holding (Fig. 5d). Furthermore, the lattice parameter of ferrite fluctuates markedly during isothermal holding at 1025 °C and during solutionizing at 1120 °C (Fig. 8). The fluctuations are more shallow at 1000 °C and vanish at lower isothermal holding temperatures where the lattice parameter of ferrite decreases smoothly.

3.3. Effect of quenching after isothermal holding

Quenching to 40 °C after isothermal holding does not lead to a significant change in the phase fraction distribution in samples held at temperatures from 800 to 950 °C where the ferrite fraction decreased below 0.5 wt% during the holding treatment. In the samples HD750 and HD1000 held at 750 and 1000 °C, respectively, which contained at the end of the holding treatment 12.9 and 8.6 wt% of ferrite, respectively, both σ phase and austenite fractions increased during quenching (Tables 3, 4). In sample HD750 γ_{sum} increased from 60.6 to 62 wt% and σ phase increased from 26.6 to 27 wt%. In sample HD1000 γ_{sum} increased from 64.9 to 66.6 wt% and σ phase increased from 26.5 to 27.6 wt%. No

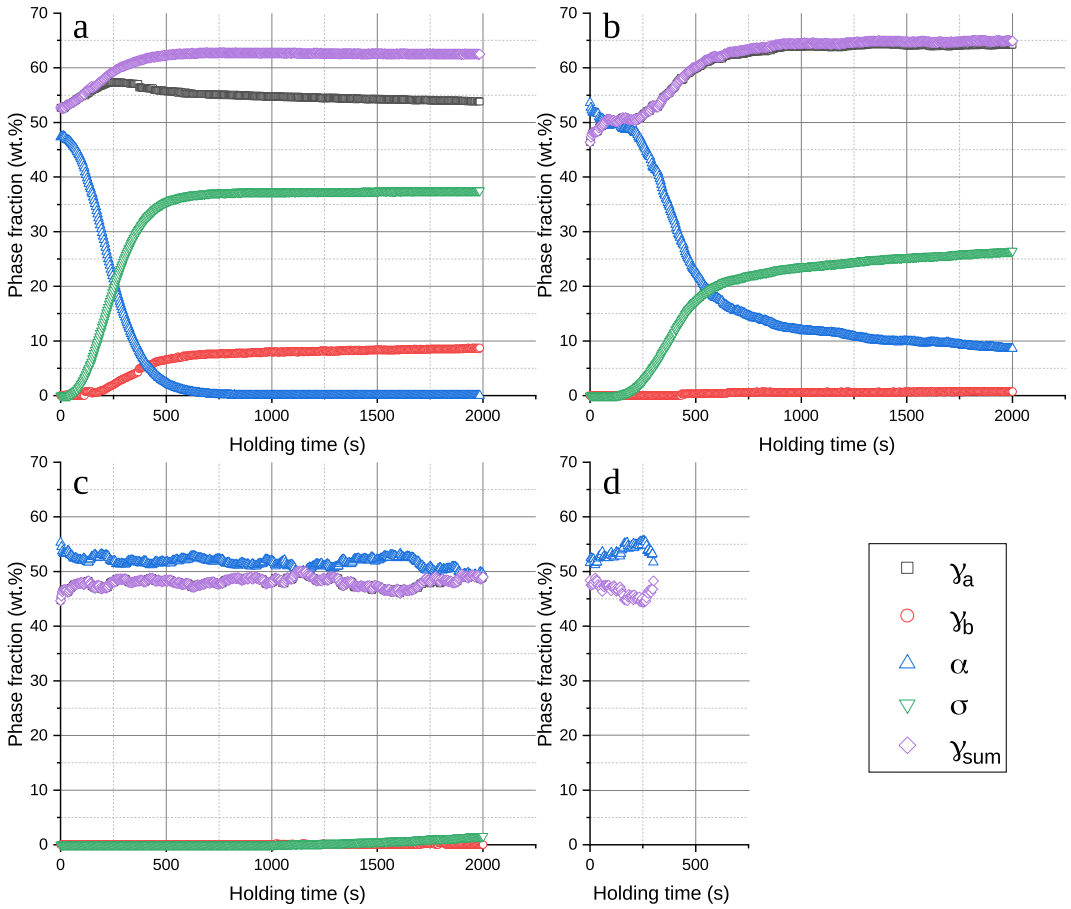

Fig. 5. Evolution of matrix phases and σ phase during during isothermal holding at (a) 800 °C, (b) 1000 °C (c) 1025 °C, and (d) 1120 °C. (a) At holding temperatures $\leq$ 950 °C the initial increase in the overall austenite fraction γ_{sum} corresponds to the fraction with the original lattice parameter γ_a. γ_b develops only with significant σ phase fraction. (b) Growth of σ phase at 1000 °C slows down at markedly higher ferrite fractions compared to lower holding temperatures. No significant fraction of γ_b develops. Austenite and ferrite fractions oscillate slightly before the onset of σ phase formation. (c) σ phase growth at 1025 °C is greatly decelerated. Ferrite and austenite fractions oscillate around ~50% phase fraction. (d) Oscillating behavior of austenite and ferrite phase fractions at 1120 °C. The corresponding plots showing the phase fraction evolution during holding at 750, 850, 900 and 950 °C are shown in the supplementary material.

Table 3
Phase fractions in wt% at the end of the isothermal holding as well the lattice parameters at the end of the isothermal holding. The lattice parameter values for α for samples HD800, HD850, HD900 and HD950, for γ_b for samples HD1000 and HD1025 and for σ phase for sample HD1025 are omitted because the respective phase fractions are too small for the lattice parameter refinement.

Name	Phase fractions (wt%)				Lattice parameters (Å)				
	α	γ_a	γ_b	σ	a(α)	a(γ_a))	a(γ_b)	a(σ)	c(σ)
HD750	12.9	53.3	7.3	26.6	2.905	3.666	3.644	8.896	4.642
HD800	0	53.8	8.7	37.5		3.671	3.651	8.907	4.649
HD850	0	46	15.6	38.5		3.675	3.657	8.917	4.655
HD900	0.3	53.4	11.7	34.6		3.677	3.661	8.928	4.661
HD950	0.3	52.6	13.3	33.7		3.679	3.668	8.935	4.667
HD1000	8.6	64.2	0.7	26.5	2.918	3.682		8.950	4.675
HD1025	49.7	48.8	0	1.5	2.924	3.689			

investigated sample shows a significant increase of the ferrite fraction during quenching through the ferrite stability field below about 650 °C.

3.4. Observations of different σ phase growth mechanisms

3.4.1. Lattice parameters and chemical composition of σ phase after quenching

The lattice parameters of σ phase after quenching are sensitive to the holding temperature during aging. The a and c lattice parameters in the sample held at 1000 °C are about 0.1% and 0.08%, respectively, larger than in the lower temperature regime (Table 4). Such a difference is not observed between the α and γ_a lattice parameters after quenching. Measurements of the chemical composition of σ phase by EPMA in samples held at 1000 °C for 600 s and 900 °C for 75 s substantiate the compositional differences. The Mo concentration in sigma phase decreases from 9.2(3) wt% in the sample held at 1000 °C to 7.9(3) wt% in the sample held at 900 °C whereas the Cr concentration decreases slightly from 30.4(2) to 29.8(2) from 1000 to 900 °C. Conversely, the Fe concentration increases slightly from 52.1(3) to 53.4(5) from 1000 to 900 °C and the Ni concentration increases from 4.3(1) to 4.7(2).

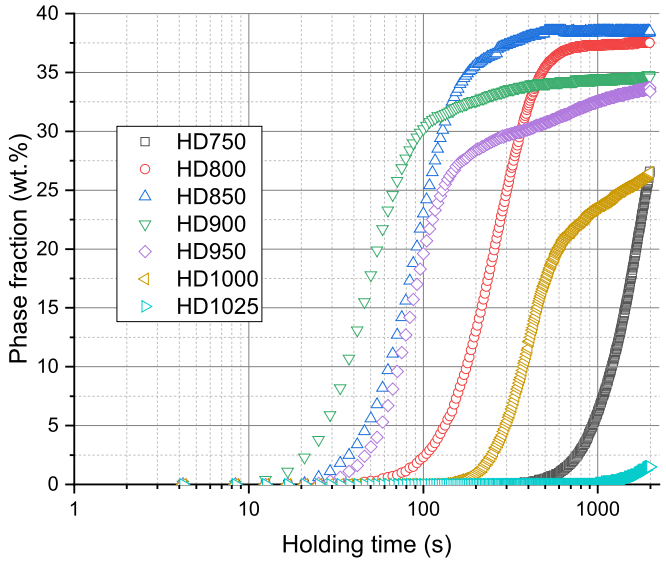

Fig. 6. Evolution of the σ phase fraction during isothermal holding at temperatures from 750 °C to 1025 °C showing characteristic sigmoidal precipitation kinetics. The fastest formation occurs at 900 °C. Samples held at 950 °C and 1000 °C show fast initial growth of σ phase and subsequently slower linear growth.

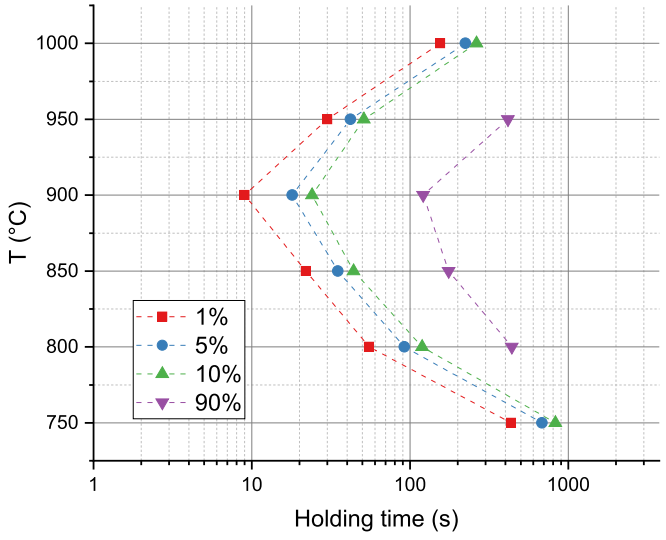

Fig. 7. Time-temperature-precipitation diagram showing the time needed for the precipitation of 1, 5, 10 and 90% of the final σ phase fraction. The final fractions for 750 °C and 1000 °C after the dissolution of ferrite were measured as 33 and 32% by image analysis from longer ex-situ holding experiments since the transformation was not completed after 2000 s at these temperatures. The nose temperature is around 900 °C. Lines are guides to the eye.

3.4.2. *Relative abundance of σ phase and austenite during holding*

The relative abundance of σ phase and the fraction of austenite that forms during holding changes during the holding treatment. To evaluate this change we define $\sigma/\Delta\gamma_{sum}(t)$ as the ratio between the σ phase fraction and the fraction of γ_{sum} that has formed between the start of the isothermal holding and time t. In the temperature range from 850 °C to 950 °C $\sigma/\Delta\gamma_{sum}$ reaches a maximum early during the holding treatment after an initial increase (Fig. 9). The initial increase of the ratio begins when σ phase starts to precipitate at ferrite/ferrite and ferrite/austenite boundaries after the austenite fraction has already increased, when the sample is cooled from the solutionizing temperature to the respective holding temperature. It subsequently decreases to a value slightly below

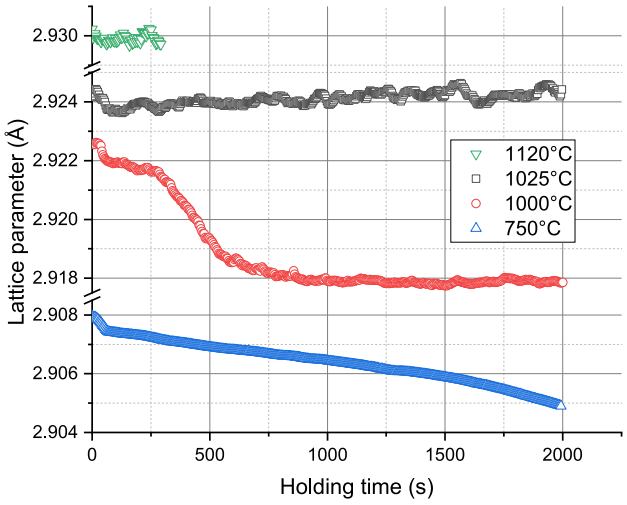

Fig. 8. Evolution of the ferrite lattice parameter during holding at 750 °C, 1000 °C, 1025 °C and 1120 °C. The oscillating behavior of the ferrite lattice parameter at 1025 °C and 1120 °C is markedly diminished at 1000 °C and absent at 750 °C. The corresponding evolution of the austenite lattice parameter is shown in the supplementary material.

the maximum value. This decrease occurs when the eutectoid decomposition of ferrite starts where secondary austenite is created alongside σ phase. At 850 °C the ratio is then constant for the rest of the holding treatment, whereas at 900 °C and 950 °C the ratio increases slowly and linearly for the duration of the holding treatment. At 900 °C the maximum is reached after 50 s and a σ phase fraction of 18 wt%, at 850 °C the maximum is reached after 170 s and a σ phase fraction of 33.8 wt% and at 950 °C the maximum is reached after 120 s at a σ phase fraction of 23.2 wt%.

3.4.3. *Ex-situ SEM analysis*

To observe the microstructural differences concomitant with the change of σ phase formation we also performed ex-situ SEM analysis on samples held for different times at 900 °C as well as one sample held at 1000 °C for 600 s (Fig. 10). The samples held at 900 °C were quenched to room temperature after 25, 50 and 75 s, respectively, which corresponds to the states before the maximum, at the maximum and shortly after the maximum, respectively in Fig. 9. The σ phase fractions obtained by image analysis from back-scattered electron images agree well with the XRD results. The obtained area fractions for the samples held at 900 °C for 25, 50 and 75 s are 3, 19 and 23%, respectively, compared to 4, 17.5 and 26.3 wt%. respectively, from the XRD results. For the sample held at 1000 °C for 600 s the obtained area fraction is about 20% and the XRD evaluation gives 20 wt%. After holding for 25 s at 900 °C and subsequent quenching σ phase precipitates are observed in the form of a few µm thick rims between ferrite/ferrite and some ferrite/austenite boundaries, while σ phase precipitates in the grain interior are not observed (Fig. 10). After 50 s i.e. at the $\sigma/\Delta\gamma_{sum}$ maximum the rims occur at most ferrite/austenite boundaries and become thicker by growing into the ferrite grains. Lamellar σ phase precipitates are prevalent in the ferrite interior and some fine grained domains of σ phase and austenite presumably formed by eutectoid transformation can be observed in ferrite grains. At a holding time of 75 s after the maximum in Fig. 9 the microstructure is similar to the microstructure observed after 50 s, but lamellar and eutectoid σ phase morphologies are observed more frequently. The sample held at 1000 °C exhibits σ phase only in the form of rims between boundaries even after 600 s, where the phase fraction of σ phase is 20 wt%.

Table 4
Phase fractions in wt% and lattice parameters after quenching to 40 °C. The values for sample HD950 are omitted because the sample was reheated above the solvus temperature of σ phase after the isothermal holding at 950 °C to dissolve the σ phase. The lattice parameters for α for samples HD800, HD850 and HD900, for γ_b for samples HD1000 and HD1025 and for σ phase for sample HD1025 are omitted because the respective phase fractions are too small for the lattice parameter refinement.

Name	Phase fractions (wt%)				Lattice parameters (Å)				
	α	γ_a	γ_b	σ	a(α)	a(γ_a))	a(γ_b)	a(σ)	c(σ)
HD750	11	51.1	10.9	27	3.620	3.601	2.875	8.797	4.585
HD800	0.3	54.2	8.3	37.2	3.621	3.599		8.798	4.585
HD850	0	48.4	13.5	38.2	3.620	3.600		8.798	4.584
HD900	0.1	50	15.7	34.2	3.619	3.604		8.802	4.586
HD1000	5.9	65	1.6	27.6	3.618		2.872	8.809	4.589
HD1025	46.9	49	2	2	3.624		2.879		

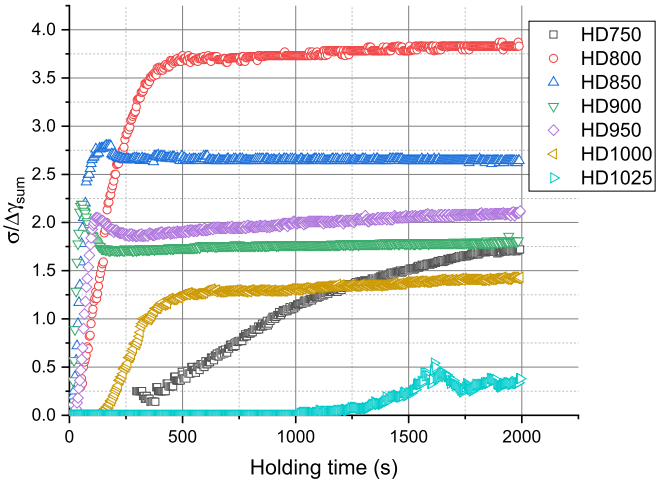

Fig. 9. Evolution of the ratio of σ phase over $\Delta\gamma_{sum}$, where $\Delta\gamma_{sum}$ is the fraction of γ_{sum} that forms during isothermal holding.

4. Discussion

4.1. Assessing σ phase formation kinetics at the nose temperature

Formation of σ phase in our experiments occurs significantly faster and the transformation has a lower nose temperature than reported in earlier experimental studies on the formation of σ phase during isothermal heat treatment of HDSS that employed ex-situ SEM analysis on quenched samples [13,14]. Kim et al. [13] investigated a HDSS with in part higher concentrations of elements promoting σ phase formation (+0.9 wt% Cr, +0.1 Si, −2.03 wt% Mo and + 3.38 wt% W). These authors proposed a longer duration than the present study, 69 s, to reach a σ phase fraction of 1 vol% at a nose temperature of 936 °C (900 °C in the present study). Zhang et al.[14] investigated the HDSS UNS S32707 which also has a slightly higher concentration of σ phase forming elements (+0.53 wt% Cr, +0.23 wt% Si and + 0.27 wt% Mo). They also reported a higher nose temperature of 950 °C than the present study with a moderately slower formation of σ phase than at the nose in the present study despite the higher alloying grade. It is notable that the investigation by Zhang et al. [14] was performed using significantly coarser microstructures with austenite lamellae of about 25 μm

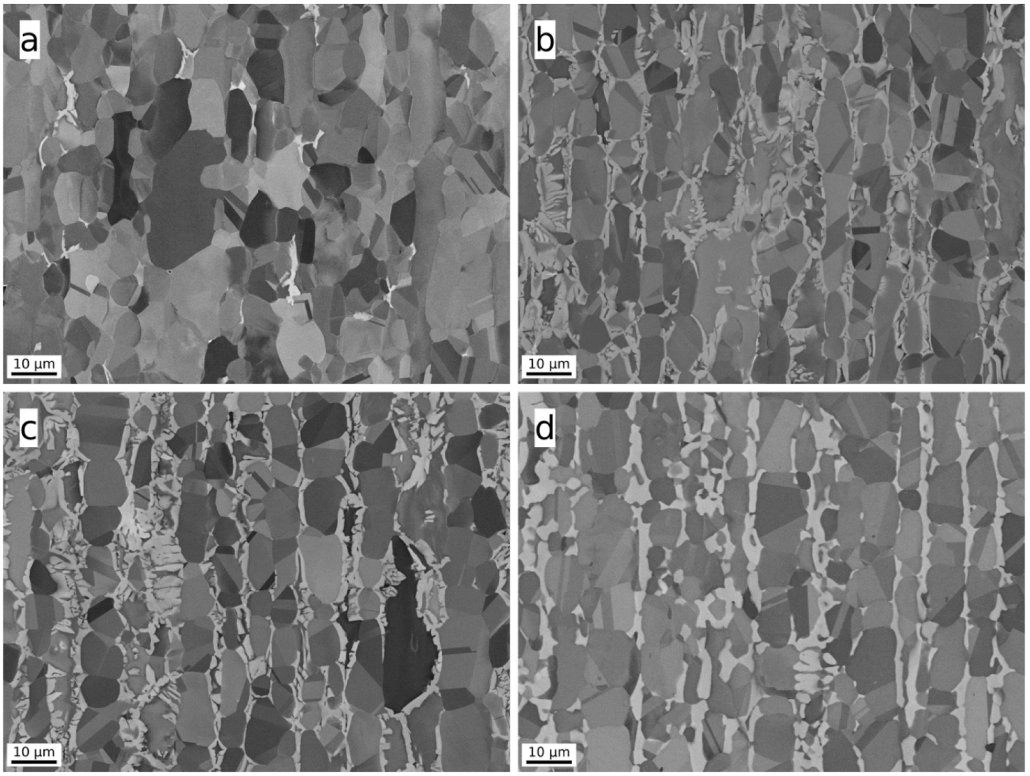

Fig. 10. Back-scattered electron images of samples held at 900 °C for (a) 25 s, (b) 50 s, and (c) 75 s, and (d) 1000 °C for 600 s. The bright regions are σ phase. Austenite grains can be identified by the frequent twin boundaries. The wire drawing direction is vertical.

thickness, where the lower ferrite/ferrite and ferrite/austenite boundary densities may delay the formation of σ phase particularly in the early stages compared to the finer microstructure in the present study. Pardal et al. [24] observed such a size effect on the kinetics of σ phase precipitation in a super duplex steel which leads to a slower onset of σ phase formation and slower growth in coarser microstructures.

Elmer et al. [16] performed an in-situ XRD study on the formation of σ phase during isothermal holding in a lower grade duplex steel using reflection geometry. They observed faster σ phase formation than in studies on similar steels that quantified the σ phase fraction by microscopy after quenching. Elmer et al. [16] argued that the apparent slower kinetics particularly in the early stage of transformation found in the studies using metallographic analysis of quenched samples may be due to the lower accuracy, poor statistics and the difficulty of observing small σ phase precipitates. On the other hand, they also cautioned that their own results might be influenced by surface effects due to the low X-ray penetration depth in their experiments. However, such an effect can be ruled out for our experiments that employed high energy X-ray diffraction of bulk samples in transmission and probed large sample volumes. Furthermore, the fast kinetics of σ phase formation in HDSS exacerbate the limitations of determining phase fractions by ex-situ metallographic techniques, since the quenching duration is long enough that substantial σ phase growth occurs in samples with significant ferrite content. Moreover, the discontinuous measurements after quenching do not allow for a sufficiently fine time resolution. These experimental constraints of ex-situ studies on precipitation kinetics especially regarding time-sensitive early stages should be recognized and taken into account in the calibration of kinetic models of precipitate formation.

4.2. Effect of moving boundaries on chemical heterogeneities at elevated temperatures

The observed oscillations of ferrite and austenite phase fractions during holding at the solutionizing temperature of 1120 °C and at 1025 °C and at the early stages of 1000 °C demonstrate that the interface boundaries between the matrix phases are not static even when no major changes in the phase fractions occur. Since the chemical compositions of ferrite and austenite in duplex steels are significantly different [4,6,18], such boundary movements necessarily lead to chemical heterogeneities at and near the boundaries, which will influence subsequent precipitation of σ phase. Chemical variations in ferrite are confirmed by the oscillations of the ferrite lattice parameter during holding between 1120 °C and 950 °C, where the amplitude of the oscillations increases with increasing temperature. These variations in the size of the ferrite lattice parameter are interpreted as changes in the average chemical composition of ferrite.

Heterogeneous distributions of σ phase forming elements such as Cr, Si and Mo that develop during solutionizing in particular in the vicinity of ferrite/austenite boundaries may play a significant role in the fast formation of σ phase in the early stages of isothermal holding. Thus it is proposed that models of σ phase precipitation in duplex steels consider that early stage precipitation occurs in ferrite regions that are not in chemical equilibrium.

4.3. Effect of σ phase formation mechanisms on precipitation kinetics

The changes of σ phase formation mechanisms with temperature and holding time need to be considered to understand σ phase formation kinetics. The absence of secondary austenite in samples held at 1000 °C and 1025 °C shows that concurrent formation of secondary austenite and σ phase becomes feasible only at temperatures below 1000 °C in our material. Jacob and Povoden-Karadeniz [18] demonstrated in their thermodynamic simulation study on a hyper-duplex steel with similar composition as in the present study that cooling from temperatures above the solvus temperature of σ phase leads to a region down to about 1000 °C where austenite, ferrite and σ phase are stable, before ferrite decomposes at temperatures $\leq$ 950 °C (see also Fig. 2). The eutectoid decomposition of ferrite into σ phase and austenite can only occur below this temperature. Consequently, the σ phase fraction formed during holding at 1000 °C has a different chemical composition indicated by larger lattice parameters than the σ phase fraction formed in the lower temperature regime and the different concentrations especially regarding Mo and Ni obtained from the EPMA measurements. Within the lower temperature regime the σ phase lattice parameter after quenching does not significantly vary between different holding temperatures. However, decreasing the holding temperature within the lower temperature regime leads to a stronger differentiation between γ_a and γ_b lattice parameters despite the lower mobility of alloying elements. This behavior is consistent with the finding of earlier studies that lower holding temperatures lead to finer σ phase precipitate morphologies (e.g. [11]).

In addition to the difference of σ phase formation mechanisms in the high and lower temperature regimes the change of σ phase formation during isothermal holding from growth at ferrite/ferrite and ferrite/austenite boundaries to eutectoid formation of σ phase and secondary austenite in ferrite needs to be taken into account for a comprehensive description of σ phase formation kinetics. For example, our results show that the assumption made in prevalent modeling approaches that σ phase precipitation occurs by fast nucleation and subsequent growth without further significant nucleation [25–27] is not realistic in the lower temperature regime and may lead to deviations of the modeled behavior from experimental evidence.

5. Conclusions

In-situ high energy X-ray diffraction experiments were performed to characterize the phase transformations in a hyper duplex stainless steel during isothermal holding from 750 °C to 1025 °C. The exceptional beam brilliance and large analyzed sample volume allowed to record high quality diffractograms with a time resolution of 4 s to precisely track the formation of σ phase.

A time transformation precipitation diagram for σ phase precipitation was calculated from the phase fractions determined by Rietveld analysis of the diffraction data. The nose temperature lies at about 900 °C which is moderately lower than the nose temperature determined in earlier studies on similar hyper duplex steels using ex-situ SEM observations of quenched samples. We found that in the present study precipitation of σ phase at the nose temperature occurs faster than at these earlier studies, despite the somewhat lower concentrations of σ phase forming elements in the present study. This discrepancy may be due to the difficulty of observing fine precipitates by microscopic methods and their lower accuracy.

The measured phase fractions of austenite and ferrite fluctuate around their equilibrium values during the solutionizing treatment at 1120 °C as well as during isothermal holding at 1000 °C and 1025 °C. This implies that austenite/ferrite boundaries at these temperatures are mobile and locally the phase composition fluctuates even when the overall phase composition is stable, leading to chemical heterogeneities near the boundaries. Likewise the ferrite lattice parameter fluctuates at these holding temperatures, which indicates the local variation of the chemical composition of ferrite with time.

While σ phase formation changes distinctly from interface controlled growth to diffusion controlled growth during holding at 1000 °C, when the nucleation sites at the boundaries are exhausted holding treatments in the lower temperature regime lead to a more gradual change from interface control to diffusion control. The changes in σ phase formation mechanisms observed by the in-situ experiments were correlated with differences in σ phase morphologies, the presence of secondary austenite and the chemical composition of σ phase.

Declaration of Competing Interest

The authors declare that they have no known conflict of interest that could have appeared to influence the work reported in this paper.

Data availability

Data will be made available on request.

Acknowledgements

The financial support by the Austrian Federal Ministry for Digital and Economic Affairs and the National Foundation for Research, Technology and Development is gratefully acknowledged. Werner Artner from the Xray-center of the TU Wien is thanked for many helpful discussions. We acknowledge voestalpine BÖHLER Edelstahl for providing the HDSS samples. We acknowledge DESY (Hamburg, Germany), a member of the Helmholtz Association HGF, for the provision of experimental facilities. Parts of this research were carried out at PETRA III and we would like to thank Norbert Schell for assistance in using beamline P07. Beamtime was allocated for proposal I-20191290 EC. The authors acknowledge TU Wien Bibliothek for financial support through its Open Access Funding Programme.

Appendix A. Supplementary data

Supplementary data to this article can be found online at https://doi.org/10.1016/j.matchar.2023.113124.

References

[1] J.O. Nilsson, Super duplex stainless steels, Mater. Sci. Technol. (UK) 8 (8) (1992) 685–700, https://doi.org/10.1179/mst.1992.8.8.685.
[2] G. Chail, P. Kangas, Super and hyper duplex stainless steels: structures, properties and applications, Procedia Struct. Integr. 2 (2016) 1755–1762, https://doi.org/10.1016/j.prostr.2016.06.221.
[3] M. Pohl, O. Storz, T. Glogowski, Effect of intermetallic precipitations on the properties of duplex stainless steel, Mater. Charact. 58 (1) (2007) 65–71, https://doi.org/10.1016/j.matchar.2006.03.015.
[4] J. Nilsson, A. Wilson, Influence of isothermal phase transformations on toughness and pitting corrosion of super duplex stainless steel saf 2507, Mater. Sci. Technol. 9 (7) (1993) 545–554.
[5] M. Knyazeva, M. Pohl, Duplex steels: part I: genesis, formation, structure, Metallogr. Microstruct. Anal. 2 (2) (2013) 113–121, https://doi.org/10.1007/s13632-013-0066-8.
[6] S. Kumar, S. Krisam, A. Jacob, F. Kiraly, A. Keplinger, R. Abart, E. Povoden-Karadeniz, Microstructures and element distributions in an aged hyper duplex stainless steel and corresponding hardness variation, Mater. Des. 194 (2020), 108951, https://doi.org/10.1016/j.matdes.2020.108951.
[7] A. Keplinger, C. Martinez, M. Hausbauer, M. Kapp, Early stages of deleterious phases in super and hyper duplex stainless steel and their effect on toughness, Berg-Hüttenmänn. Monatsh. 165 (1) (2020) 33–39, https://doi.org/10.1007/s00501-019-00936-4.
[8] M. Pohl, O. Storz, Sigma-phase in duplex-stainless steels, Int. J. Mater. Res. 95 (7) (2004) 631–638, https://doi.org/10.3139/146.017999.
[9] R. Magnabosco, Kinetics of sigma phase formation in a duplex stainless steel, Mater. Res. 12 (3) (2009) 321–327, https://doi.org/10.1590/S1516-14392009000300012.
[10] G.S. da Fonseca, P.S.N. Mendes, A.C.M. Silva, Sigma phase: nucleation and growth, Metals 9 (1) (2019) 34, https://doi.org/10.3390/met9010034, 2019, Vol. 9, Page 34.
[11] M. Pohl, O. Storz, T. Glogowski, σ-phase morphologies and their effect on mechanical properties of duplex stainless steels, Zeitschrift fuer Metallkunde/Mater. Res. Adv. Tech. 99 (10) (2008) 1163–1170, https://doi.org/10.3139/146.101738.
[12] M.V. Biezma, U. Martin, P. Linhardt, J. Ress, C. Rodríguez, D.M. Bastidas, Non-destructive techniques for the detection of sigma phase in duplex stainless steel: a comprehensive review, Eng. Fail. Anal. 122 (Apr 2021), https://doi.org/10.1016/j.engfailanal.2021.105227.
[13] S.M. Kim, J.S. Kim, K.T. Kim, K.T. Park, C.S. Lee, Effect of Ce addition on secondary phase transformation and mechanical properties of 27Cr–7Ni hyper duplex stainless steels, Mater. Sci. Eng. A 573 (2013) 27–36, https://doi.org/10.1016/j.msea.2013.02.044.
[14] B. Zhang, Z. Jiang, H. Li, S. Zhang, H. Feng, H. Li, Precipitation behavior and phase transformation of hyper duplex stainless steel UNS S32707 at nose temperature, Mater. Charact. 129 (2017) 31–39, https://doi.org/10.1016/j.matchar.2017.04.018.
[15] A. Jacob, E. Povoden-Karadeniz, Predictive computations of intermetallic σ phase evolution in duplex steel. (II) Thermo-kinetic simulation in duplex and hyper duplex stainless steels, Calphad 71 (2020), 101810, https://doi.org/10.1016/j.calphad.2020.101810.
[16] J.W. Elmer, T.A. Palmer, E.D. Specht, Direct observations of sigma phase formation in duplex stainless steels using in-situ synchrotron X-ray diffraction, Metall. Mater. Trans. A Phys. Metall. Mater. Sci. 38 (3) (2007) 464–475, https://doi.org/10.1007/s11661-006-9076-3.
[17] J.W. Elmer, T.A. Palmer, E.D. Specht, In situ observations of sigma phase dissolution in 2205 duplex stainless steel using synchrotron X-ray diffraction, Mater. Sci. Eng. A 459 (1–2) (2007) 151–155, https://doi.org/10.1016/j.msea.2007.01.071.
[18] A. Jacob, E. Povoden-Karadeniz, Predictive computations of intermetallic σ phase evolution in duplex steel. (I) Thermodynamic modeling of σ phase in the Fe–Cr–Mn–Mo–Ni system, Calphad 71 (2020), 101998, https://doi.org/10.1016/j.calphad.2020.101998.
[19] E. Povoden-Karadeniz, mc_fev2.059, URL, https://www.matcalc.at/index.php/databases/open-databases, 2016.
[20] N. Schell, A. King, F. Beckmann, T. Fischer, M. Müller, A. Schreyer, The high energy materials science beamline (HEMS) at PETRA III, Mater. Sci. Forum 772 (2014) 57–61.
[21] A.P. Hammersley, FIT2D: an introduction and overview, in: ESRF Internal Report ESRF97HA02, 1997.
[22] M. Wojdyr, Fityk: a general-purpose peak fitting program, J. Appl. Crystallogr. 43 (5–1) (2010) 1126–1128.
[23] T. Degen, M. Sadki, E. Bron, U. König, G. Nénert, The highscore suite, Powder Diffract. 29 (S2) (2014) S13–S18.
[24] J.M. Pardal, S.S. Tavares, M.C. Fonseca, J.A. de Souza, R.R. Côrte, H.F. de Abreu, Influence of the grain size on deleterious phase precipitation in superduplex stainless steel UNS S32750, Mater. Charact. 60 (3) (2009) 165–172, https://doi.org/10.1016/j.matchar.2008.08.007.
[25] A.T. Kempen, F. Sommer, E.J. Mittemeijer, Determination and interpretation of isothermal and non-isothermal transformation kinetics; the effective activation energies in terms of nucleation and growth, J. Mater. Sci. 37 (7) (2002) 1321–1332, https://doi.org/10.1023/A:1014556109351, 2002 37:7.
[26] P. Ferro, F. Bonollo, A semiempirical model for sigma-phase precipitation in duplex and superduplex stainless steels, Metall. Mater. Trans. A 43 (4) (2011) 1109–1116, https://doi.org/10.1007/S11661-011-0966-7, 2011 43:4.
[27] P. Ferro, A. Fabrizi, J.-O. Nilsson, Research and reports on metals intermetallic phase precipitation in duplex stainless steels: considerations on the use of Johnson-Mehl-Avrami-Kolmogorov equation, Technol. Med. 1 (2017).